

X-rays from accretion shocks in T Tauri stars: The case of BP Tau

J.H.M.M. Schmitt¹, J. Robrade¹, J.-U. Ness², F. Favata³, B. Stelzer⁴

¹ Hamburger Sternwarte, Gojenbergsweg 112, D-21029 Hamburg, Germany

² University of Oxford, Department of Theoretical Physics, 1 Keble Road, Oxford OX1 3NP, United Kingdom

³ Astrophysics Division, ESA/ESTEC, P.O. Box 299, 2200 AG, Noordwijk, The Netherlands

⁴ Dipartimento di Scienze Fisiche e Astronomiche, Università di Palermo, Piazza del Parlamento 1, I-90134 Palermo, Italy

Received / Accepted

Abstract. We present an XMM-Newton observation of the classical T Tauri star BP Tau. In the XMM-Newton RGS spectrum the O VII triplet is clearly detected with a very weak forbidden line indicating high plasma densities and/or a high UV flux environment. At the same time concurrent UV data point to a small hot spot filling factor suggesting an accretion funnel shock as the site of the X-ray and UV emission. Together with the X-ray data on TW Hya these new observations suggest such funnels to be a general feature in classical T Tauri stars.

Key words. X-rays: stars – stars: individual: BP Tau – stars: pre-main sequence, coronae, activity – accretion

1. Introduction

One of the central results of stellar X-ray astronomy is the discovery that all “cool stars”, i.e., stars with outer convective envelopes, are surrounded by hot coronae (Schmitt & Liefke, 2004). The usual interpretation of this finding is that the combined action of turbulence in the outer convection zones and the ever-present rotation leads to dynamo action with vigorous production of magnetic fields and ensuing activity. X-ray observations support this interpretation with the “onset of activity”, i.e., the rapid increase in X-ray detection rates of main sequence stars at spectral type $\approx F0$ and the correlation between rotation rate and activity.

Strong X-ray emission is found also from many young stars such as zero age main sequence stars or T Tauri above the main sequence. Both flavors of T Tauri stars, i.e., the weak line T Tauri stars (wTTS) without disks as well as the classical T Tauri stars (cTTS) with disks are X-ray sources (Feigelson & Montmerle, 1999). The presence of a disk around cTTS constitutes a fundamental difference compared to a “normal” star without disk, since the energy stored in the disk material can be released through accretion and lead to superphotospheric and/or time variable emissions; in fact, the optical variability observed in (some) cTTS (Gullbring et al., 1996) is commonly interpreted in this fashion. Yet the high-energy activity observed from cTTS and wTTS is usually interpreted as a “scaled-up” version of solar activity. The low-resolution X-ray data available prior to XMM-Newton and *Chandra* made a distinction between the X-ray properties of wTTS and cTTS very difficult; while some differences in emission level and variability properties between wTTS and cTTS were indicated by statistical studies (Stelzer et al., 2000; Stelzer & Neuhäuser,

2001; Flaccomio et al., 2003), a characterization of the physical properties of the X-ray emitting regions was impossible.

This situation has changed with the advent of high-resolution grating spectroscopy with XMM-Newton and *Chandra*. A great surprise was the X-ray spectrum of the cTTS TW Hya (Kastner et al., 2002; Stelzer & Schmitt, 2004), which clearly showed low forbidden to intercombination (f/i) line ratios in the O VII and Ne IX triplets, which were interpreted as due to high plasma densities in the X-ray emitting regions. The extensive spectral survey by Ness et al. (2004), who studied high-resolution X-ray spectra of 48 coronal sources, provided no star that would even come close to the low O VII f/i-ratio as observed for TW Hya. Clearly, TW Hya differs in its coronal properties from all other stars, and it is very natural to ascribe this difference to the presence of an accretion disk around TW Hya. Specifically, Kastner et al. (2002) and Stelzer & Schmitt (2004) interpret the X-ray emission as arising from an accretion shock produced by matter falling down onto TW Hya along a magnetic funnel. There is an obvious need to examine further cTTS with high-resolution spectroscopy in order to assess whether TW Hya’s X-ray properties are typical for cTTS or not. We therefore obtained a high-resolution X-ray spectrum of the cTTS BP Tau with the Reflection Grating Spectrometer (RGS) onboard XMM-Newton, and the purpose of this letter is to present and discuss the implications of this observation.

2. Observations

2.1. The cTTS BP Tau: Optical and X-ray properties

An extensive overview of the optical properties of BP Tau is given by Gullbring et al. (1996) and Errico et al. (2001). Its

spectral type varies from K5-K7, it rotates fast ($v \sin(i) = 15.4$ km/sec), but various rotation period measurements varying between 6.1 to 8.3 days have been published. The cTTS nature of BP Tau is clearly demonstrated by the excess continuum (veiling) and Balmer emission (Bertout et al., 1988). There is debate about BP Tau’s distance, and Wichmann et al. (1998) argue against BP Tau being an outlier from the Taurus-Auriga cloud as suggested by its HIPPARCOS parallax. From extensive optical monitoring Gullbring et al. (1996) conclude that optical variability is common in BP Tau, but in character very much different from variability encountered in typical flare stars. Most of the observed changes are slow and smooth and are interpreted as the result of inhomogeneous accretion from the disk onto the stellar surface. This view is strongly supported by the circular polarization in the He I λ 5876 emission line measured by Johns-Krull et al. (1999), who deduce a mean longitudinal magnetic field of 2460 ± 120 G in the line forming region and argue that accretion occurs preferentially along large-scale magnetic loops with a small filling factor. X-ray emission from BP Tau at a level of $\approx 10^{30}$ erg/sec was first reported by Walter & Kuhl (1981) using the *Einstein Observatory*. In a simultaneous optical and X-ray observations of BP Tau with ROSAT Gullbring et al. (1997) found no evidence for correlated variations between the two bands and thus attributed the X-ray emission to magnetically active regions.

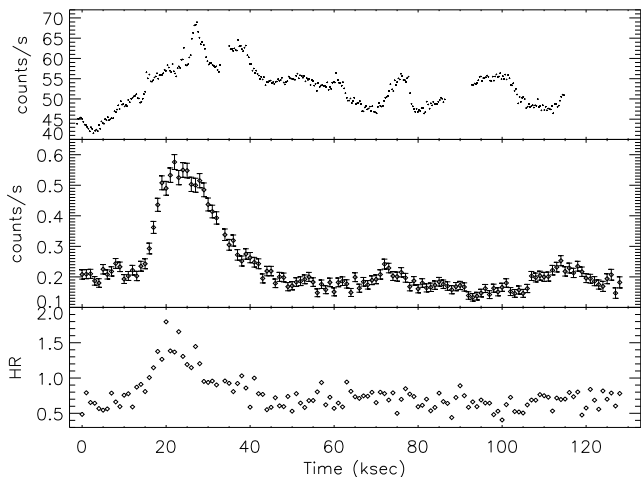


Fig. 1. OM UVW1 light curve (upper panel; bin size 300 sec), EPIC PN X-ray light curve (medium panel), and X-ray hardness ratio defined as ratio between the rates in the bands 0.2-1.0 and 1.0-10.0 keV (lower panel; both with bin size 1000 sec).

2.2. XMM-Newton X-Ray Data

BP Tau was observed with XMM-Newton on August 15, 2004 for a duration of 131 ksec (obs-id 0200370101) with the RGS as prime instrument. The observations were performed in full-frame mode employing the thick filter for both the MOS and the PN cameras of the European Photon Imaging Camera (EPIC). The optical monitor (OM) was operated using the UVW1 filter with a band pass between 2500 Å and 3500 Å and an effective wavelength of 2910 Å according to the XMM-Newton

users’ handbook (Ehle et al. (2004)). All XMM-Newton data was analyzed with SAS version 6.0. Background conditions were very quiet throughout most of the BP Tau observation and only 10 ksec of data had to be screened. In Fig. 1 we show the EPIC PN X-ray light curve, the X-ray hardness ratio (lower panel), and the UVW1 light curve (upper panel). An obvious X-ray flare with a spectral hardness increase occurred between $\approx 20 - 40$ ksec into the observations; the X-ray flare may be accompanied by a much longer lasting UV event, but there is no strict correlation between X-ray and UV variability.

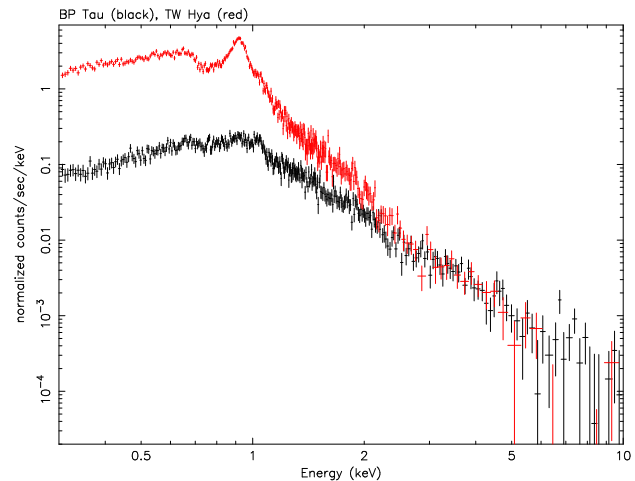


Fig. 2. EPIC PN spectrum of BP Tau (quiescent phase; lower black points) in comparison to the EPIC PN spectrum of TW Hya (upper, red/grey points)

In Fig. 2 we show the EPIC PN spectrum of BP Tau (lower curve) in comparison to TW Hya (upper curve; cf. Stelzer & Schmitt, 2004). Above ≈ 2.5 keV the two spectra overlap, while at lower energies the flux of TW Hya exceeds that of BP Tau by almost an order of magnitude. Spectral modeling of the EPIC PN spectrum using simple multi-temperature fits requires absorption column densities of $1 - 2 \times 10^{21}$ cm $^{-2}$ depending on the chosen model and consistent with the relation between N_H and E_{B-V} (Jenkins & Savage, 1974); hot temperatures (≈ 2 keV) are required in contrast to TW Hya, whose EPIC spectrum is dominated by cool plasma of ≈ 0.3 keV (cf., Stelzer & Schmitt, 2004). Thus the EPIC spectra of BP Tau and TW Hya suggest differences between the two stars.

However, BP Tau’s instrumental background-subtracted high resolution RGS2 spectrum looks rather similar to that of TW Hya, (cf., Fig. 3); probing the lower-energy plasma it shows mostly oxygen and neon lines with – at best – weak iron lines as well as signs of a continuum. Because of the low signal only a few spectral lines can be reliably detected in our RGS spectra. The clearly detected lines include the O VII Ly α line, the O VII triplet, the Ne X Ly α line, and the Ne IX triplet at 13.5 Å; interestingly, no unambiguous RGS detections of iron lines, in particular at 15.03 Å and 17.07 Å were obtained (cf., Fig. 3 and Table 1), reminiscent of the low amount of iron derived for TW Hya. Also, no lines of nitrogen and carbon could be detected, presumably because of the larger absorption column towards

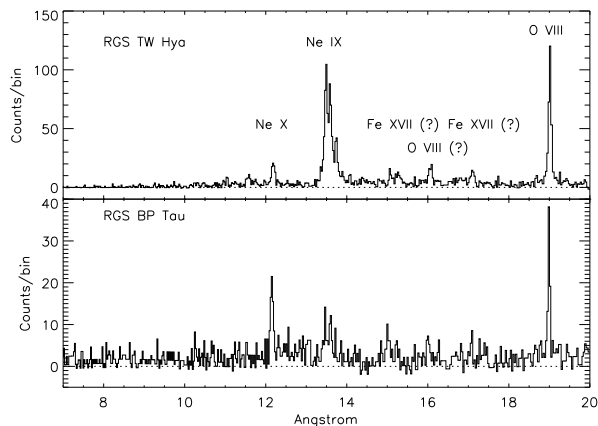


Fig. 3. Comparison of instrumental background subtracted RGS2 spectra of TW Hya and BP Tau with line identifications.

BP Tau. The detected lines together with the derived best fit line counts and their errors are listed in Table 1; all line counts were derived with the CORA program (Ness & Wichmann, 2002), assuming Lorentzian line shapes. The line fits were carried out in such a way that the wavelength differences between the triplet lines and line widths were held constant; the background was adjusted by eye, different choices of background lead to line flux variations well within the errors; in Fig. 4 we plot the RGS spectrum around the O VII triplet at 22 Å together with our best fit model. From the numbers listed in Table 1 we find an observed f/i -ratio of 0.37 ± 0.16 for O VII and 0.40 ± 0.26 for Ne IX; the latter assumes negligible contamination by iron, which is a severe problem for the interpretation of any Ne IX triplet data (cf., Ness et al., 2003) depending on the strength of the iron lines.

Line ID	λ (Å)	Counts	Error	Instr.	Flux
Ne x Ly α	12.14	91.5	11.7	RGS2	13.2
Ne ix He r	13.46	37.0	9.9	RGS2	5.2
Ne ix He i	13.56	31.2	9.8	RGS2	4.4
Ne ix He f	13.71	12.5	7.1	RGS2	1.7
O viii Ly β	16.03	25.8	6.4	RGS1	4.1
O viii Ly β	16.00	16.7	6.2	RGS2	2.3
O viii Ly α	18.97	95.5	11.4	RGS2	14.2
O vii He r	21.6	47.7	8.6	RGS1	8.9
O vii He i	21.8	36.6	7.8	RGS1	7.1
O vii He f	22.1	13.7	5.5	RGS1	2.7
Fe xvii	15.03	< 20		RGS1	< 2.9

Table 1. X-ray lines detected in the RGS spectrum of BP Tau, line counts and photon fluxes in units of 10^{-6} ph s $^{-1}$ cm $^{-2}$

3. Discussion

Stelzer & Schmitt (2004) interpret the XMM-Newton X-ray data on the cTTS TW Hya in terms of an accretion funnel scenario, where the X-ray emission is emitted in a shock (“hot spot”) produced by the infall of material along the magnetic field at essentially free-fall velocity onto the stellar surface.

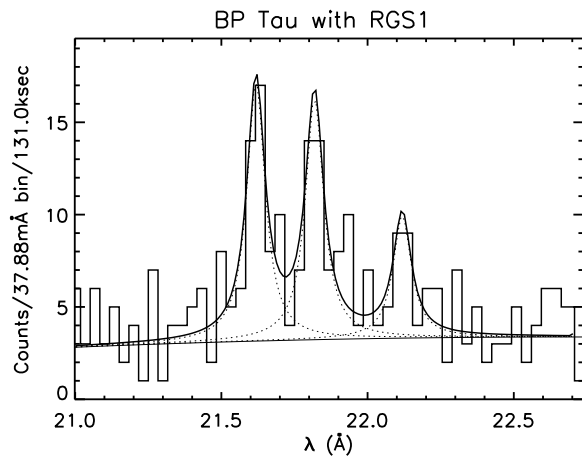


Fig. 4. RGS spectrum BP Tau: O VII triplet region with best fit model.

Does the same scenario also apply to the cTTS BP Tau and possibly to cTTS as a class ?

It is instructive to compare the observed line fluxes from BP Tau with those measured from TW Hya (cf., Table 2 in Stelzer & Schmitt, 2004), taking into account the different amounts of interstellar absorption. For ISM columns of 3×10^{20} cm $^{-2}$ and 1×10^{21} cm $^{-2}$ respectively, we compute ISM transmissivities of (0.83, 0.54) at 18.97 Å, (0.77, 0.42) at 21.6 Å, (0.93, 0.78) at 12.14 Å, and (0.91, 0.73) at 13.46 Å for TW Hya and BP Tau respectively. These values lead to ratios between the Ly α and He-like r flux ratios 1.9 and 2.1 for oxygen and 0.3 and 2.7 for neon respectively. While the ratios for oxygen are about similar, those for neon differ quite significantly, thus the emission measure distribution in BP Tau must also be different. We also note that the Ly α and He-like r flux ratios observed in BP Tau for oxygen and neon are not consistent with a single temperature.

Line	low state	high state	“low state”/3.2
Ne x Ly α	48.6 ± 8.7	42.7 ± 8.0	15.2 ± 2.7
O viii Ly α	59.2 ± 9.1	32.5 ± 6.6	18.5 ± 2.8
O vii He r	34.4 ± 7.3	10.7 ± 4.1	10.8 ± 2.3
O vii He i	24.6 ± 6.3	9.5 ± 4.2	7.7 ± 2.0
O vii He f	5.5 ± 3.8	5.6 ± 3.2	1.7 ± 1.2

Table 2. Line counts measured in “low state” and in “high state” and extrapolated “high state” counts.

We next checked to what extent individual RGS-detected lines are influenced by the flare. We defined a “high state” by including all data recorded in the time interval 13.5 - 43.0 ksec (counted from the start of the observations as in Fig. 1) and a “low state” including all the rest and determined line counts as before. We also computed the expected number of “high state” counts extrapolating from the “low state” values and list all results in Table 2. Clearly, within the errors the O VII line counts are unaffected by the flaring emission, and only 15 % of the recorded O VIII line counts can be attributed to the flare; for Ne X this contribution rises to 30 %. We thus conclude that the

observed O VII emissions are not significantly affected by the flare, while O VIII Ly α is contaminated by < 20 %.

In addition to the X-ray data concurrent photometric UV data from the XMM-Newton OM are available for BP Tau (cf., Fig. 1). The UV continuum flux of BP Tau is thought to be produced by an accretion hot spot as demonstrated by Ardila & Basri (2000) and Errico et al. (2001). The same applies of course also to our OM UVW1 photometric data, which would require filling factors of ten or more stellar surfaces if they were to be reconciled with BP Tau’s photospheric temperature. We therefore assume in the following that the recorded UVW1 flux is exclusively produced in a hot spot and deredden this UV-flux using $A_V = 0.51$ (Gullbring et al., 1998) and $E_{B-V} = 0.32 \times A_V$. Without any further spectral information we assume an emergent blackbody spectrum with variable temperature T_{em} , convert count rate into specific energy flux (erg/cm²/s/Å) using the instrumental conversion factor of 4.4×10^{-16} (erg/cm²/count/Å), and compute the fractional surface area and filling factor required to account for the (dereddened) observed UVW1 flux. Assuming hot spot temperatures between 8000 - 10000 K (cf., Calvet & Gullbring, 1998; Ardila & Basri, 2000), we invariably find filling factors between 0.6 – 4%, which are in line with values computed from more sophisticated models including shocks and an irradiated photosphere (Calvet & Gullbring, 1998).

Converting the observed oxygen f/i-ratio of 0.37 ± 0.16 to density yields a nominal value of $\log n_e = 11.48$ with a (formal) error range of (11.3-11.8), neglecting radiative deexcitation of the forbidden line level; therefore the derived densities may be regarded as upper limits if the X-ray emitting region is affected by the observed UV radiation. We re-emphasize that both BP Tau and TW Hya have lower f/i-ratios and higher densities than all of the coronal X-ray sources analyzed by Ness et al. (2004). If the O VII f/i-ratio was contaminated by a lower density “coronal component”, any accretion-related shock component would require an even smaller f/i-ratio.

Assuming optically thin emission, the observed energy flux in the O VII and O VIII lines, f_{oxy} , is given by $f_{oxy} = A_{sh} n_e^2 P_{oxy} / 4\pi d^2$, where A_{sh} , z , n_e , P_{oxy} denote shock area, cooling zone thickness, electron density and line cooling function respectively. The post shock plasma cooling time τ is given by $\tau = 3n_e kT / n_e^2 P_{tot}$, with k , T and P_{tot} denoting Boltzmann’s constant, temperature and overall radiative loss function. Postshock velocity V_{post} , z and τ are related through $\tau = z / V_{post}$. Thus we calculate the mass accretion rate $M_{acc} = \frac{4\pi d^2 f_{oxy} m_H \mu P_{tot}}{3kT_{oxy}}$, with m_H denoting hydrogen mass and μ the mean molecular weight. With the observed values for f_{oxy} we find with $T = 2.5$ MK $M_{acc} \approx 9 \times 10^{-10} M_{\odot}/yr$, about an order of magnitude smaller than inferred at UV wavelengths; since the observed oxygen fluxes may contain non-accretion related contributions, this value of M_{acc} should be considered as an upper limit. Filling factors of a few percent yield densities consistent with the O VII triplet and a cooling zone thickness of ≈ 100 km. As to the depth of the X-ray emitting region, a model independent absorption estimate using the observed photon flux ratio in the Ly α and Ly β lines of 3.1 (cf., Table 1) requires with temperature of $\log T = 6.8$ an equivalent absorption column of

$\approx 5 \times 10^{21} \text{ cm}^{-2}$. Given the large errors on the Ly β /Ly α photon flux ratio and the internal consistency between RGS2 values and optical extinction and the N_H values of $N_H \approx 2 \times 10^{21} \text{ cm}^{-2}$ derived from the broad band X-ray spectra, we conclude that there is no real evidence for an “additional” absorption of BP Tau’s X-ray flux.

4. Conclusions

The XMM-Newton RGS spectrum clearly demonstrates that X-ray emitting O VII layers in the cTTS BP Tau are either at high density and/or immersed in a strong ultraviolet flux. Both possibilities can be well explained by an X-ray emitting accretion shock on BP Tau. This accretion shock can, however, produce only the low-temperature components in the broad band X-ray spectra of BP Tau (and TW Hya); to explain the high temperature component additional processes possibly involving magnetic interactions between the disk and the star or magnetic activity anchored in the photosphere are required. Also, the derived mass accretion rates are smaller than those inferred from optical and UV data, but a detailed modeling in particular taking into account non-equilibrium effects is still lacking. At any rate, the XMM-Newton observations of BP Tau show that TW Hya is not “alone”. Accretion shocks at the end of magnetic funnels connecting disk and stellar surface may in fact be a common feature of cTTS stars as a class.

Acknowledgements. This work is based on observations obtained with XMM-Newton, an ESA science mission with instruments and contributions directly funded by ESA Member States and the USA (NASA). JR and JUN acknowledge support from DLR under grant 50OR0105 and PPARC under grant PPA/G/S/2003/00091.

References

- Ardila, D., R., Basri, G.S. 2000, ApJ, 539, 834
 Bertout, C., Basri, G.S., Bouvier, J. 1998, ApJ, 330, 350
 Calvet, N. & Gullbring, E. 1998, ApJ, 509, 802
 Ehle, M., Breitfellner, M., Gonzales Riestra, M., et al. 2004, XMM-Newton User’s Handbook
 Errico, L., Lamzin, S. A., Vittone, A. A., 2001, A&A, 377, 557
 Gullbring, E., Barwig, H., Chen, P.S., Gahm, G.F., Bao, M.X. 1996, A&A, 307, 791
 Gullbring, E., Barwig, H., Schmitt, J.H.M.M. 1997, A&A, 324, 155
 Gullbring, E., Hartmann, L., Briceño, C., Calvet, N. 1998, ApJ, 492, 392
 Feigelson, E.D. & Montmerle, T. 1999, Ann.Rev.A&A, 37, 363
 Flaccomio, E., Micela, G., Sciortino, S. 2003, A&A, 402, 277
 Jenkins, E.B., Savage, B.D. 1974, ApJ, 187, 243
 Johns-Krull, C.M., Valenti, J.A., Hatzes, A.P., & Kanaan, A. 1999, ApJ, 510, L41
 Kastner, J.H., Huenemoerder, D.P., Schulz, N.S., & Canizares, C.R. 2002, ApJ, 567, 434
 Ness, J.-U. & Wichmann, R. 2002, AN, 323, 129
 Ness, J.-U., Brickhouse, N.S., Drake, J.J., & Huenemoerder, D.P. 2003, ApJ, 598, 1277
 Ness, J.-U., Güdel, M., Schmitt, J.H.M.M., et al. 2004, A&A, 427, 667

- Schmitt, J.H.M.M. & Liefke, C. 2004, *A&A*, 417, 651
Stelzer, B., Neuhäuser, R. & Hambaryan, V. 2000, *A&A*, 356, 949
Stelzer, B. & Neuhäuser, R. 2001, *A&A*, 377, 538
Stelzer, B. & Schmitt, J.H.M.M. 2004, *A&A*, 418, 687
Walter, F.M & Kuhi, L.V. 1981, *ApJ*, 284, 194
Wichmann, R., Bastian, U., Krautter, J., Jankovics, I., & Rucinski, S.M. 1998, *MNRAS*, 301L, 39